J Mater Sci (2016) 51:4538–4548
DOI 10.1007/s10853-016-9766-1

A first-principles lattice dynamical study of type-I, type-II, and type-VIII silicon clathrates

Payam Norouzzadeh[1] · **Charles W. Myles**[2]

Received: 24 November 2015 / Accepted: 19 January 2016 / Published online: 29 January 2016
© Springer Science+Business Media New York 2016

Abstract The pristine crystalline type-I, type-II, and type-VIII silicon clathrates have been studied using state of the art first-principles calculations based on density functional theory and density functional perturbation theory. We apply quasi-harmonic approximation to study structural stability, the possibility of temperature or pressure-driven phase transitions, along with Grüneisen parameters, coefficients of thermal expansion and thermal conductivities to estimate the degree of phonon anharmonicity for selected silicon clathrates. It is shown that a pressure-driven phase transition between type-I and type-II silicon clathrates may occur, and a temperature-driven phase transition between type-I and type-VIII Si clathrates at high temperature is likely. We further show that the relatively high Grüneisen parameters (1.5, 1.65, and 1.29, respectively for Si_{46}-I, Si_{136}-II, Si_{46}-VIII), the existence of negative regions in the thermal expansion coefficient curves and very low thermal conductivities all indicate that the phonon anharmonicity in these silicon clathrates is high.

Introduction

Silicon material systems have been studied extensively for decades and have a broad range of technological applications. According to the phonon glass-electron crystal concept by Slack [1] in 1995 the interest on the cage-like silicon clathrates as promising thermoelectric (TE) materials considerably increased. The most important characteristic of TE is the figure-of-merit $ZT = S^2\sigma T/\kappa$ (here S is the Seebeck coefficient, T is the temperature, σ is the electrical conductivity, and κ is the thermal conductivity). However, applicability of TE materials is affected by other material characteristics such as thermal and mechanical properties. Therefore, having deep insight into these physical properties of pristine silicon clathrates as parent materials through atomistic level studies warrants a flawless design of derivative materials for TE purposes (Fig. 1).

Most investigation on Si clathrates to date has dedicated on the synthesis and characterization, and transport properties. However, work on their fundamental properties such as thermal, vibrational, elastic, and thermodynamic ones remains restricted. Phonon anharmonicity arises from phonon–phonon interactions and affects the thermal properties of materials. For example, it contributes to the negative thermal expansion of Si clathrates [2]. Therefore, the concept of phonon anharmonicity has a key role in the TE materials design.

To quantify the anharmonic interactions within a lattice, the values of physical effects such as thermal conductivity, coefficient of thermal expansion (CTE) and Grüneisen parameter can be used. The CTE cannot be explained by harmonic theory of the lattice as the phonon frequency does not depend on the amplitude of the vibrations [3]. The thermal resistivity requires phonon anharmonicity as harmonic phonons would never be scattered, so a perfect crystal would have infinite thermal conductivity in the whole temperature range. One solution is to accept that phonons can scatter other phonons and it occurs only if the harmonic approximation is discarded. Moreover, if the

✉ Payam Norouzzadeh
payam.norouzzadeh@okstate.edu

[1] School of Electrical and Computer Engineering, Helmerich Advanced Technology Research Center, Oklahoma State University, 74106 Tulsa, OK, USA

[2] Department of Physics, Texas Tech University, Lubbock, TX 79409-1051, USA

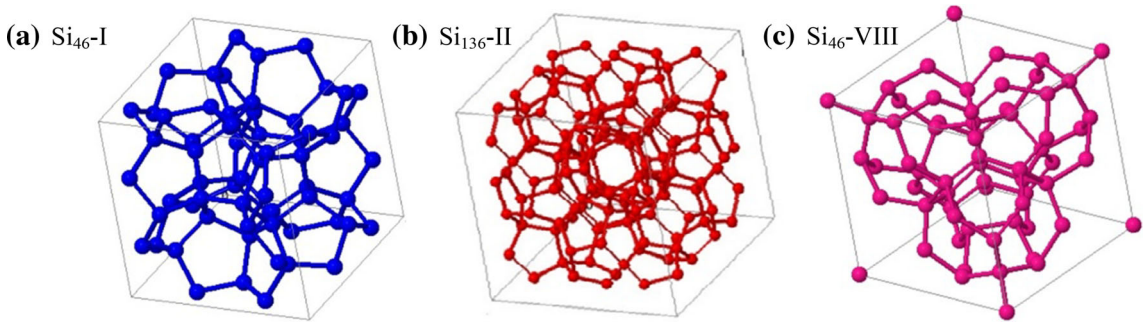

Fig. 1 Schematic representation of conventional unit cells for **a** type-I, **b** type-II, and **c** type-VIII silicon clathrates

lattice potential is harmonic, the phonon frequencies are volume-independent, and the derivative of phonon frequency with respect to the volume is zero at all temperatures. So, the Grüneisen parameter that will be defined later, is related to the anharmonicity of phonons. In case of clathrates, the anomalous motion of rattler atoms residing inside the cage can be considered as an extra reason for phonon anharmonicity [4–6]. It has been shown that the ionic radius of the guest atoms and the cage size crucially affect the phonon anharmonicity and in turn the thermal conductivity in clathrates [7, 8]. In general, quantifying the phonon anharmonicity is a difficult task and in the present study we use Grüneisen parameter, coefficient of thermal expansion, and thermal conductivity to evaluate it. In this study, we assume that the anharmonic contributions beyond quasiharmonicity are negligible and employ quasiharmonic approach (QHA) for calculations.

The primary purpose of this work is to present and discuss the phase stability, possibility of pressure or temperature-driven phase transitions, and anharmonicity of three pristine silicon clathrates Si_{46}-I, Si_{136}-II, and Si_{46}-VIII by employing a first-principles approach. We use the density functional theory (DFT), and present the properties calculated from dynamical properties: an analysis of phonon dispersions and density of states, of Grüneisen parameters, of thermal expansion coefficients, and finally a study of the lattice thermal conductivity of Si_{46}-I, Si_{136}-II, and Si_{46}-VIII clathrate materials utilizing Slack's model [9].

Theoretical background and computational methodology

Crystal structure

Clathrates can be considered as cage-like polyhedrons with shared faces. The guest-included clathrates built up from a framework lattice in which encapsulates the lattice of guest atoms. The sp^3-type covalent bindings link the atoms together. Clathrates can be doped either by intercalation until one atom in each cage, which corresponds to 20 % of doping, or by substituting atoms in the framework. The type-I silicon clathrate, namely, Si_{46}-I, has a simple cubic lattice with 46 atoms per unit cell and the $Pm\bar{3}n$ (Hermann–Mauguin notation) No. 223 group symmetry (see Table 1). The type-II silicon clathrate Si_{46}-II, has 34 atoms in its primitive unit cell in which belongs to the face-centered-cubic (fcc) $Fd\bar{3}m$ No. 227 symmetry space group. The type-VIII silicon clathrate, called Si_{46}-VIII, is a body-centered cubic lattice with 23 atoms in its primitive unit cell and the $I\bar{4}3m$ No. 217 symmetry. Type-I clathrates consist of dodecahedra (E_{20}) and tetrakaidekahedra (E_{24}) polyhedral [10] while type-II clathrates form dodecahedra and hexadecahedra (E_{28}) [11]. Type-VIII clathrates are comprised only one pent agonal dodecahedra [12]. Table 1 presents the symmetry and Wyckoff sites for each clathrate structure.

Table 1 Symmetry and Wyckoff positions of type-I, type-II, and type-VIII clathrates

Si_{46}-I ($Pm\bar{3}n$: No 223)		Si_{136}-II ($Fd\bar{3}m$: No 227)		Si_{46}-VIII ($I\,I\bar{4}3m\ 3\ m$: No 217)	
6c	x = 0.25, y = 0, z = 0.5	8a	x, y, z = 0.125	2a	x, y, z = 0
16i	x, y, z = 0.684	32e	x, y, z = 0.217	8c	x, y, z = 0.384
24 k	x = 0, y = 0.883, z = 0.692	96 g	x, y = 0.0575, z = 0.3705	12d	x = 0.25, y = 0.5, z = 0
				24 g	x, y = 0.585, z = 0.143

Computational methodology

The DFT-based QUANTUM-ESPRESSO package was employed to perform calculations [13]. The generalized gradient approximation, through the Perdew-Burke-Ernzerhof parameterization [14] and norm-conserving Troullier-Martins [15] pseudopotentials factorized in Kleinman–Bylander form [16] have been used. The Brillouin zone has been sampled by a $4 \times 4 \times 4$ Monkhorst–Pack grid for structural optimization [17]. The Kohn–Sham wave functions are expanded using a standard plane wave basis set with a kinetic energy cutoff of 30 Rydbergs. The structures are relaxed until the largest force becomes less than 10^{-3} eV/Å and the calculations are converged to 10^{-7} eV/cell. Using the linear response theory of the DFT, the dynamical matrix, Born effective charges, and dielectric constants were computed to calculate phonon frequencies in the Brillouin zone [18, 19]. A $4 \times 4 \times 4$ q grid was employed for static properties with $6 \times 6 \times 6$ k grid mesh, and 30 Rydbergs of energy cutoff to obtain the force constants matrices and achieve the inverse Fourier transformation. Thermal expansion is indirectly taken into account through performing calculations for several lattice constant around the equilibrium one.

The phonon calculations have been conducted using the small displacement method as implemented in the phon package [20]. The GGA have been used to describe the exchange–correlation effects [14]. The projector-augmented wave (PAW) potentials have been used with the cutoff energy up to 450 eV. Integration over the Brillouin zone was performed using a special k-points technique [17] with $4 \times 4 \times 4$ mesh together with Methfessel-Paxton smearing of 0.2 eV [21]. A supercell which is a single unit cell was used in all calculations due to the large unit cell of selected clathrates (~ 10 Å).

Our approach is distinct from the similar studies [2, 22] as they have applied the LDA method to calculate the temperature dependency of lattice constant and CTE for clathrates while we have utilized the GGA method.

Anharmonicity

Anharmonic effects originate from phonon–phonon interactions, and these interactions arise from the cubic or quartic terms in the phonon potential. To understand the thermal transport properties and thermodynamic stability of TE materials at higher temperatures, having a good insight into anharmonic effects is essential [23]. Phonon anharmonicity causes entropy of materials to increase at elevated temperatures, and shorten the phonon lifetimes which in turn leads to finite phonon mean free paths. However, a few studies of non-harmonic effects in Si clathrates have been reported [2, 22].

Although, anharmonicity has been studied extensively [24] a method in which incorporates the anharmonicity in free energy is still lacking. As explained earlier, anharmonicity contributes in coefficient of thermal expansion, Grüneisen parameter, and thermal conductivity. So, to evaluate the degree of anharmonicity in selected Si clathrates, we conduct first-principles calculations to obtain mode Grüneisen parameters, CTEs, and thermal conductivity within QHA. The anharmonicity resulted from the phonon–phonon interaction is ignored by QHA approximation. QHA considers the volume dependence of frequencies but neglects the effect of temperature on frequencies. In fact, the QHA is known to fail for materials that are stabilized at finite temperatures, since anharmonic effects are not incorporated in the computational procedure. However, assuming that the anharmonic contributions beyond quasiharmonicity are negligible, we used QHA for calculations.

Quasi-harmonic approximation

To calculate the vibrational contributions in the free energy and making finite temperature predictions, we need to compute the vibrational free energy F_{vib} and add it to the ground state energy U_0 resulted from DFT:$F(T,V) = U_0(V) + F_{\text{vib}}(T,V)$. The F_{vib} is derived from the phonon density of states as the following

$$F_{\text{vib}}(T) = k_{\text{B}}T \int_0^{\infty} \left[\frac{1}{2}\hbar\omega + k_{\text{B}}T \ln\left(1 - e^{-\frac{\hbar\omega}{k_{\text{B}}T}}\right)\right] g(\omega)\,\mathrm{d}\omega,$$

where $g(\omega)$ is the phonon density of states, and k_{B} is the Boltzmann's constant. $F_{\text{vib}}(T,V)$ is calculated for several lattice constants around the equilibrium one. By fitting the data with third-order Birch–Murnaghan equation of state,[1] the equilibrium lattice constant can be determined at each temperature assuming that $\partial B/\partial P = \text{const.}$ where B and P are isothermal bulk modulus and pressure, respectively. By calculations for various lattice constants the thermal expansion is indirectly taken into account. However, at the level of QHA the anharmonicity is ignored. By employing the QHA, we can obtain entropy of vibration, and specific heat at constant volume at finite temperature from phonon density of states with various lattice volumes.

Elastic constants

In cubic systems, the elastic tensor has three independent elastic constants namely, C_{12}, C_{22}, and C_{44}. The elastic

[1] The Birch-Murnaghan equation of state for the energy E as a function of volume V reads $E(V) = E_0 + 9/8(BV_0)[(V_0/V)^{2/3} - 1]^2 \{1 + [(4 - B')/2][1 - (V_0/V)^{2/3}]\}$. E, E_0, V, V_0, B and B' are the energy, minimum energy, the volume, volume at the minimum energy, the bulk modulus and its pressure derivative, respectively.

constants can be extracted from vibrational acoustic dispersion slopes as the following.

$$v_{\mathrm{l}}^{[100]} = \sqrt{\frac{C_{11}}{\rho}}, \quad v_{\mathrm{t}}^{[100]} = \sqrt{\frac{C_{44}}{\rho}},$$
$$v_{\mathrm{l}}^{[111]} = \sqrt{\frac{C_{11} + 2C_{12} + 4C_{44}}{3\rho}},$$

where $v_{\mathrm{l}}^{[100]}$, $v_{\mathrm{t}}^{[100]}$, $v_{\mathrm{l}}^{[111]}$, and ρ are longitudinal and transverse velocities of the sound along [100] direction, longitudinal sound velocity along [111] direction, and the density, respectively. To further explore the properties of phonons, the Debye temperature θ_{D} can be derived from the average sound velocity v_s using the following equations:

$$\frac{1}{v_{\mathrm{s}}^3} = \frac{1}{3}\left(\frac{1}{v_{\mathrm{l}}^3} + \frac{2}{v_{\mathrm{t}}^3}\right), \quad \theta_D = \frac{h}{k_{\mathrm{B}}}\left(\frac{3}{4\pi V_{\mathrm{a}}}\right)^{1/3} v_{\mathrm{s}},$$

where h and k_{B} are Planck's and Boltzmann's constants and V_{a} is the atomic volume.

Grüneisen parameter

The phonon process dominant in thermal conductivity of crystalline materials at temperatures above 1/3 the Debye temperature is the Umklapp process, in which the phonon momentum is changed by a reciprocal lattice vector. This process originates from the anharmonicity of atomic interactions and harmonic force constants [25]. In this study, we investigate on the Grüneisen parameter as one measure to estimate the anharmonicity strength of the atomic interactions in selected materials. The overall Grüneisen parameter is defined as

$$\gamma = \frac{\sum_{k,i} \gamma_{k,i} c_{v,i}(k)}{\sum_{k,i} c_{v,i}(k)}, \quad c_{v,i}(k) = \frac{\hbar\omega_i(k)}{V}\frac{\partial}{\partial T}\left[\frac{1}{e^{\hbar\omega_i(k)/k_{\mathrm{B}}T} - 1}\right]$$

in which $c_{v,i}(k)$ is the contribution of the mode (k, i) to the volumetric specific heat c_v and $\gamma_{k,i}$ are the mode Grüneisen parameters which describe the relative shift of phonon frequency of the mode (k, i) with the change of the volume. In the Debye approximation, all the normal-mode frequencies scale linearly with the Debye temperature, and therefore the overall Grüneisen parameter is given by [3]

$$\gamma = \langle \gamma_{i,k} \rangle = -\left\langle \frac{V\partial\omega_i(\kappa)}{\omega_i(\kappa)\partial V} \right\rangle,$$

where the mode is indicated by the wave vector k and the branch i. The angular frequency and the volume are represented by ω, and V, respectively.

Thermal expansion coefficient

It is well-known that anharmonic phonon–phonon interactions in diamond silicon cause to negative thermal expansion in the T = 0–150 K range. We employ the QHA to study the temperature variation of thermal expansion coefficient. At all temperatures, LDA systematically underestimates lattice constants and coefficients of thermal expansion, whereas GGA overestimates them [26]. The linear CTE is defined as

$$\alpha_{\mathrm{L}} = \frac{1}{3}\frac{1}{V_0}\frac{\partial V}{\partial T} = \frac{1}{3B}\sum_{i,k} c_{v,i}(k)\gamma_i(k),$$

where V is the volume, V_0 is the equilibrium volume, T is the absolute temperature, and B is the bulk modulus. The second expression in terms of mode Grüneisen parameters is obtained within QHA [3].

Thermal conductivity

Various phonon scattering mechanisms are involved in determination of lattice thermal conductivity. We assume that the heat is conducted only by acoustic phonons and Umklapp processes are dominant in phonon scatterings and use Slack's model [9] to compare the thermal conductivities of selected silicon clathrates. This formula has been used successfully to predict the thermal conductivity of many materials [27]. The lattice thermal conductivity in Slack's model can be written as

$$K_{\mathrm{L}} = \frac{A\bar{M}\theta_D^3\delta n^{1/3}}{\gamma^2 T},$$

where $\bar{M}$ is the average atomic mass, θ_{D} is the acoustic Debye temperature, δ^3 is the average volume per atom, n is the number of atoms in each primitive cell, γ is the Grüneisen parameter, T is the absolute temperature and A is a numerical coefficient in which Julian [28] determined an expression for it as $A = \frac{2.43\times10^{-6}}{\left(1 - \frac{0.514}{\gamma} + \frac{0.228}{\gamma^2}\right)}$. The Debye temperature and Grüneisen parameter have central role in determination of the magnitude of lattice thermal conductivity and can be calculated from the first-principles methods such as density functional theory. The three parameters $M, \theta_{\mathrm{D}}, \delta$ represent the harmonic properties, and bonding strength and moreover, are related to the average group velocities of acoustic phonons. At very low temperatures, the acoustic phonon modes are dominant in determining the thermal conductivity of materials and as temperature raises the contribution of the acoustic phonon modes in thermal conductivity reduces while the excited optical phonon modes start to contribute more. Therefore, as the temperature increases, the Debye temperature decreases

initially and reaches a minimum value $\theta_{D,min}$ at a specific temperature. The $\theta_{D,min}$ is a good approximation for the high temperature limit of the acoustic-phonon-associated Debye temperature. Beyond that specific temperature, and due to simultaneous reduction of acoustic phonon modes and increment of optical phonon modes contributing in thermal conductivity, the Debye temperature increases with temperature. The lower limit of acoustic-mode Debye temperature can be calculated from the classical definition of the lower limit for the Debye temperature θ_{min} in which is estimated from specific heat as the following

$$\theta_{D,\min} = \theta_{\min} n^{-1/3}.$$

θ_D is independent of n and therefore to express the n-dependency of the lattice thermal conductivity, the Slack's formula can be rewritten as

$$K_L = \frac{A\bar{M}\theta_D^3\delta}{\gamma^2 T n^{2/3}}$$

Results and discussion

Structure stability and phase transition

Table 2 lists the calculated lattice constants, formation energies, and the bulk moduli for the optimized silicon clathrates. The energy-volume curves were fitted to the Birch-Murnaghan equation of state (Footnote 1) to obtain the equilibrium lattice constants at $T = 0$, and the bulk moduli. The electronic energy of formation refers to the electronic part of the formation energy with respect to the elements in their standard state. The electronic part of the formation energies were calculated from the equation:

$$E_f(Si_n) = E_{Si_n} - nE_{Si},$$

where E_{Si} is the electronic energy per Si atom in diamond structure, and n is the number of atoms in the primitive unit cell. The formation energy determines if it is energetically favorable for a material to form in comparison with the solids formed by its constituents. All the calculated energies of formation are positive indicating that the selected structures are not more stable than their constituents and the chemical reaction of formations are endothermic. In fact, the formation reactions need extra energy to be initiated. It is also seen that the formation energy increases as the number of atoms in the primitive unit cell grows. Our calculated formation energies and bulk moduli considering that GGA underestimate them compared to LDA are consistent with previous theoretical study [29].

We examined the ground state structural stability of selected silicon clathrates at zero temperature and pressure and compared them with that of diamond-structured silicon (*d*-si). As the volume change is very small in an ambient pressure the solid–solid phase transitions can be studied with Helmholtz free energy instead of Gibbs free energy. Figure 2a depicts the calculated total energy versus volume for the type-I, type-II, and type-VIII silicon clathrates and

Table 2 The calculated values of lattice constants (a), bulk moduli (B), and formation energies (E_f) for the studied clathrate structures

	a (Å)	B (GPa)	E_f (kJ/mol)
Si_{46}-I	10.229	78.5	6.01
Si_{136}-II	14.7225	80.1	5.06
Si_{46}-VIII	10.1015	80.3	7.84

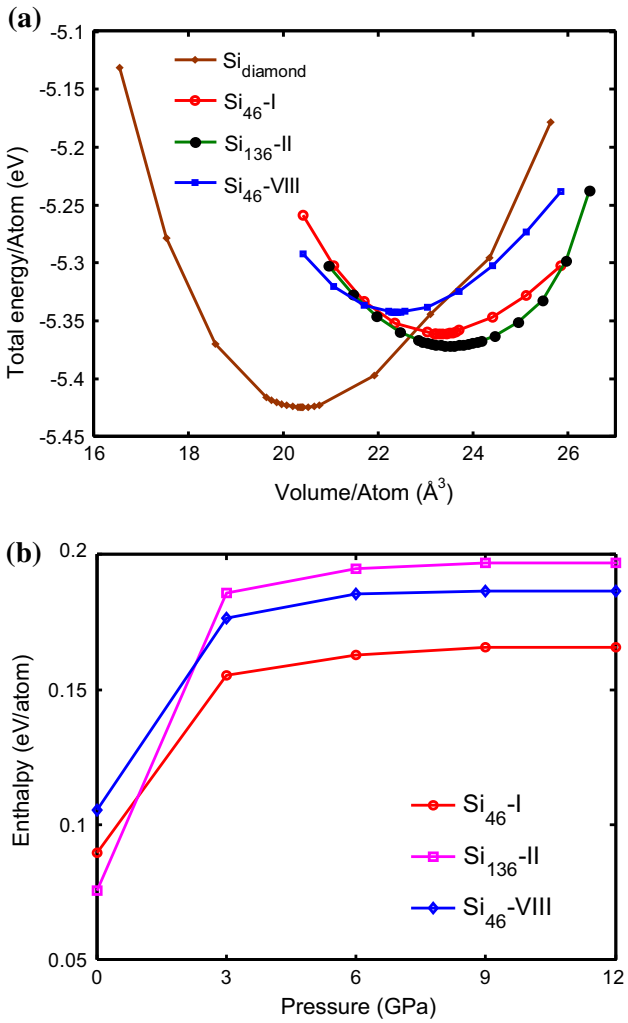

Fig. 2 **a** Energy per atom versus volume per atom of four silicon phases: diamond, clathrate-I, clathrate-II and clathrate-VIII. The data obtained from GGA-PBE calculations and is fitted with the Birch-Murnaghan equation of state. The curves of clathrates are on the right of the diamond phase. **b** Enthalpy versus pressure at room temperature obtained with the GGA method for the type-I, type-II, and type-VIII silicon clathrates

for the diamond phase of silicon as well. It is revealed that compared to *d*-si, all clathrate structures can be considered as metastable structure. Among considered silicon clathrate structures, the Si_{136}-II has the most stable ground state due to its lower energy while that of the Si_{46}-VIII has higher ground state energy. It is notable that, the relative structural stability of clathrates originates from two types of distortions. First, the small angle distortions in hybridized *sp* [3] orbitals and second the elasticity of the bond-bending distortion modes [30, 31]. Figure 2a shows a crossing of three energy-volume curves at ~ 21.9 Å^3 with the volume compression so, the structural phase transition from Si_{46}-I to Si_{136}-II and Si_{46}-VIII may occur with compression of the lattice under hydrostatic pressure. To investigate the effect of pressure on structural stability and possible phase transitions under pressure the enthalpies ($H = U + PV$) were calculated.

Figure 2b illustrates the enthalpy for the three selected silicon clathrates as a function of hydrostatic pressure calculated at room temperature using QHA. The structure in which has the lowest enthalpy is the most stable. A crossing of two enthalpy-pressure curves is a sign for a pressure-driven phase transition. The calculated results indicate that the enthalpies of all selected clathrate structures increase as the pressure raises. However, the curve slopes show that enthalpy of the Si_{136}-II increases faster than that of Si_{46}-I and Si_{46}-VIII. The enthalpy data show that Si_{46}-I is always more stable than the Si_{46}-VIII as its enthalpy curve is lower than that of Si_{46}-VIII at the whole range of pressure. So, increment of the hydrostatic pressure cannot lead to phase transition from Si_{46}-I to Si_{46}-VIII. The phase transition can occur at curve crossings. In fact, for those pressures where the enthalpies of two phases are equal, and no phase has a lower enthalpy a phase transition is possible. Figure 2b depicts that the enthalpy curve of Si_{136}-II crosses those of Si_{46}-I and Si_{46}-VIII curves at ~ 1, and ~ 2 GPa, respectively. The second crossing point (~ 2 GPa) cannot lead to a phase transition as the Si_{46}-I phase has a lower enthalpy. However, the lower crossing point shows that a pressure-driven phase transition from Si_{136}-II phase to Si_{46}-I phase may happen. Nevertheless, a thorough analysis of the effect of temperature and elastic stability is required to establish a better understanding of crystal structure.

Next, to evaluate the possibility of a temperature-driven phase transition between Si_{46}-I and Si_{46}-VIII phases the Helmholtz free energies were calculated for several lattice constants around the equilibrium one to obtain the minimum lattice constant at each temperature. Figure 3a, and b show the Helmholtz free energies of Si_{46}-I and Si_{46}-VIII structures versus lattice constant at temperatures from 0 to 1400 K at increments of 100 K. The points on the $T = 0$ curves in the above plots were obtained by DFT-based

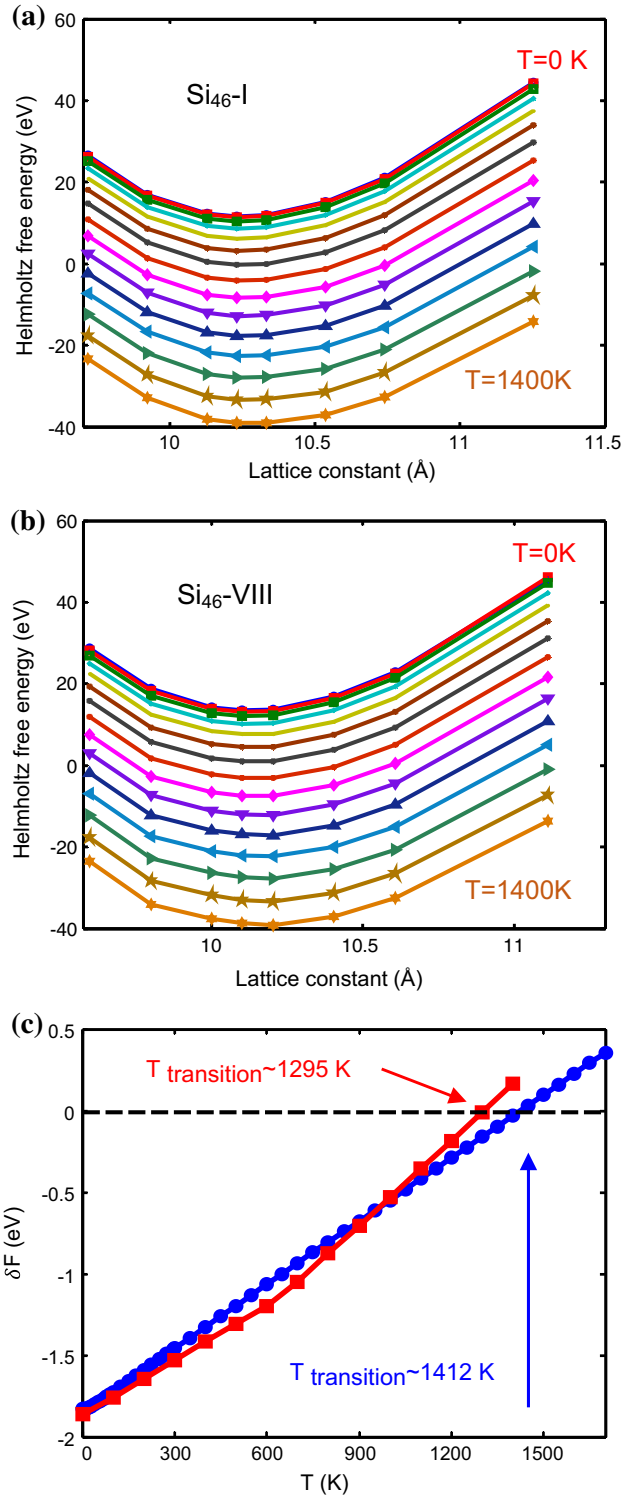

Fig. 3 Volume versus Helmholtz free energy curves are at increments of 100 K between 0 and 1400 K for **a** Si_{46}-I and **b** Si_{46}-VIII clathrates. **c** A comparison between two methods for calculation of Helmholtz free energies to obtain the temperature-driven phase transition: the QHA which does not account anharmonicity directly (*red curve*) and the minimization of free energy over several lattice constants around the equilibrium one which takes into account the anharmonicity directly (*blue curve*)

lattice dynamical calculations (phonon calculations) and their equivalent points on $T > 0$ curves were obtained using QHA. By adopting this approach, we were able to minimize the Helmholtz free energy over several lattice constants around the equilibrium one at each selected temperature and indirectly incorporate the effect of thermal expansion on lattice constant. Figure 3c demonstrates the curves of Helmholtz free energy difference between Si_{46}-I and Si_{46}-VIII structures. The blue curve represents the results of harmonic approximation in which does not into account the effect of thermal expansion while the red curve shows the results for the quasi-harmonic approximation which incorporates the effect of thermal expansion. The calculated transition points (1412 and 1295 K) are both very high and close to the melting point which is expected to be same as or near the melting point of the diamond phase of silicon (1711 K). Therefore, the temperature-driven transition between Si_{46}-I and Si_{46}-VIII structures is likely and possibly can be exploited to synthesize the hypothetical clathrate phase of silicon Si_{46}-VIII.

Phonon dispersion and density of states

Figure 4 depicts the phonon dispersions along high symmetry paths in the first Brillouin zone and phonon density of states with arbitrary unit for Si_{46}-I, Si_{136}-II, Si_{46}-VIII. The phonon dispersions were computed by diagonalizing the dynamical matrices. The clathrate structures Si_{46}-I, Si_{136}-II, Si_{46}-VIII show very similar phonon dispersions and phonon density of states compared to each other. In all the studied silicon clathrates the sharp features of the phonon density of states (PDOS) are observed which are corresponding to the relatively flat bands. The flatness of dispersion bands of silicon clathrates in the region of transverse acoustic modes which are related to the long range interactions [32], has been reported already [29]. Our calculated results are in good agreement with the previously reported empirical and theoretical studies [2, 22]. It is observed that for the studied structures the optical modes are locate within three bands. The low-frequency band varies from 2 to 6 THz for Si_{46}-I, Si_{136}-II structures while for the Si_{46}-VIII it ranges within 3-6 THz. The medium-frequency band which is the broadest one in all cases spreads over 6-12.8 THz for Si_{46}-I, Si_{136}-II, and 6-12.4 THz for Si_{46}-VIII. The high-frequency band locate within frequency ranges 12.8–14 and 12.4–15.5 THz, respectively, for Si_{46}-I, Si_{136}-II, and Si_{46}-VIII. The low- and high-frequency bands are narrow and relatively flat. The phonon bandwidth of Si_{46}-I, Si_{136}-II structures spread almost over the 0-14 THz while Si_{46}-VIII has a broader range and extends to $\sim$15.5 THz. The broader phonon bandwidth of Si_{46}-VIII provides more channels to conduct the heat and compared to other two structures a higher thermal conductivity can be expected. A common feature observed in PDOS is high PDOS values within the frequency range of 3-6 THz for the studied materials. As another common feature, the structures show phonon band gaps at frequency ranges of 12.93 to 13.21, 12.7 to 13.13, and 12.17 to 12.54 THz, with the phonon band gap values around 0.28, 0.43, and 0.37 THz, respectively, for Si_{46}-I, Si_{136}-II, and Si_{46}-VIII.

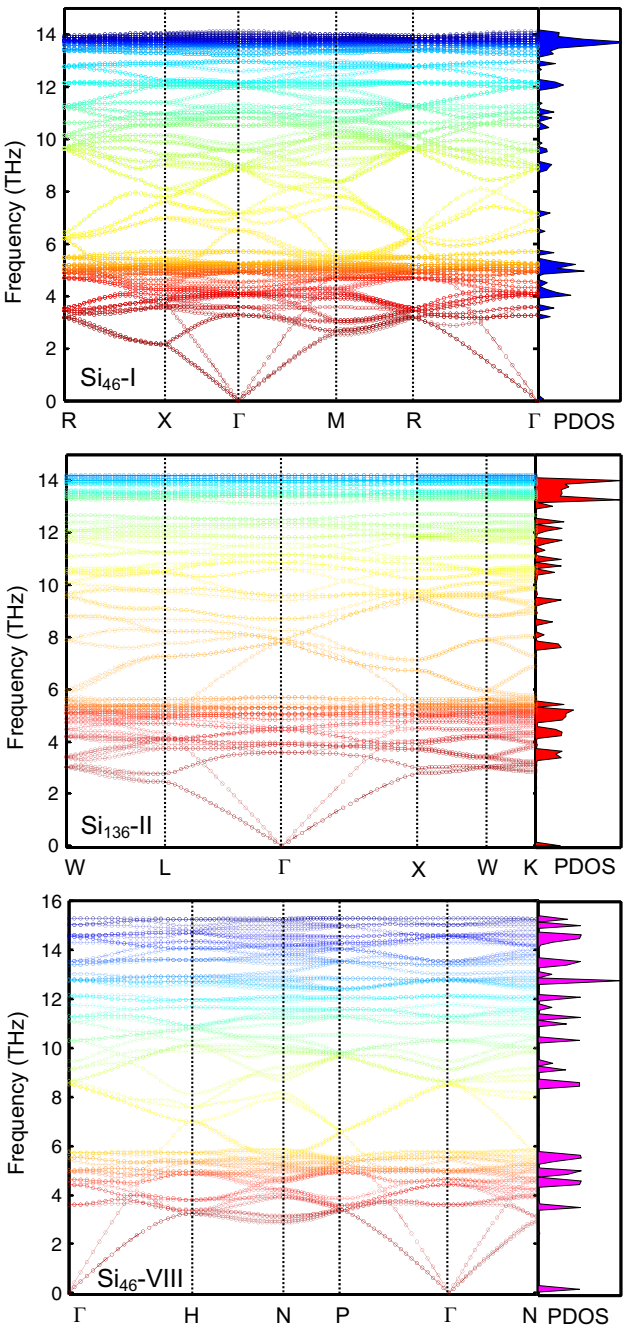

Fig. 4 Phonon dispersions along high symmetry paths in the first Brillouin zone and phonon density of states with arbitrary unit for studied silicon clathrates

Anharmonicity measures

Grüneisen parameters

In order to have deeper insight into the anharmonic effect, we calculated the mode Grüneisen parameters as the volume derivative of the phonon frequencies on a 6 × 6 × 6 mesh of reciprocal space points in which corresponds to actual k-spacing of 0.1 per angstrom. The k-mesh was forced to be centered on the gamma point. Figure 5 shows the calculated Grüneisen parameters depending on the frequency for the GGA functional. The overall Grüneisen parameter is more appropriate in this study for further calculation of thermal conductivity. The negative Grüneisen parameters are observed when the phonon frequency is under 190, and 200 cm^{-1}, equal to 5.7, and 6 THz, respectively, for Si_{136}-II, and Si_{46}-VIII clathrates. The threshold of 190 cm^{-1} is valid for the Si_{46}-I clathrate as well. However, an exception around 245 cm^{-1} (7.34 THz) is seen. Considering that other researchers have used local density approximation, our calculated Grüneisen parameters (by GGA) are in agreement with the previous theoretical studies [2, 22]. Contrast to the *d*-Si, in which the distribution of the mode Grüneisen parameters versus frequency shows symmetric features, the Grüneisen parameters of the studied silicon clathrates represent a broader spectrum at low frequencies, especially for the Si_{46}-I material.

Coefficients of thermal expansion

We used the results of our calculated GGA lattice constants to predict CTE of Si_{46}-I, and Si_{46}-VIII clathrates. We also calculated the CTE of diamond silicon to establish validity of our calculations as well. The results are presented in Fig. 6. In all three studied structures the CTE curves are similar. Our calculations reveal that all studied silicon clathrates have negative CTE with a minimum in 60-80 K temperature range [33]. However, the calculated values for the CTEs change versus temperature with different curve slopes. While the CTE values of Si_{46}-I and Si_{136}-II structures are larger than that of *d*-si, the Si_{46}-VIII phase has a smaller CTE.

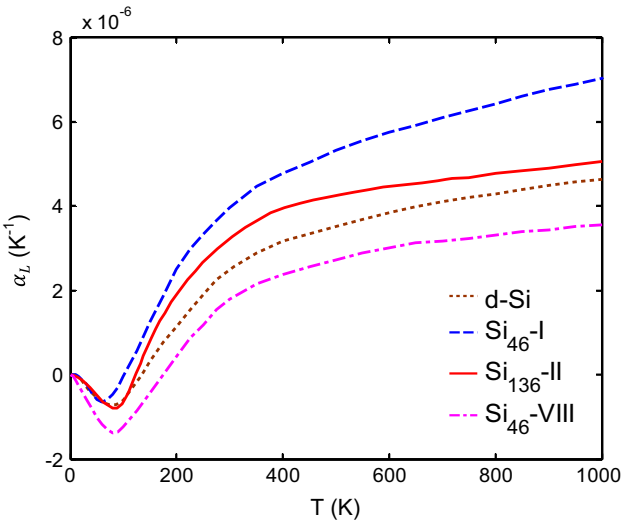

Fig. 6 The calculated coefficients of linear thermal expansion using GGA for studied Si clathrates versus temperature

It is notable that, according to a general trend for calculations within the GGA framework, the calculated values of α_L are expected to overestimate the experimental α_L. Our calculated CTE for *d*-Si is in very good agreement with the experimental result. All the calculated CTEs exhibit a region of negative thermal expansion (NTE). Such a region of NTE is well-known experimentally for the *d*-Si. According to our results the minima of NTE regions are located at 80, 60, 80, and 76 K, respectively, for *d*-Si, Si_{46}-I, Si_{136}-II, and Si_{46}-VIII in which are in very good agreement with a similar theoretical study [2]. The NTE of selected Si clathrates can be attributed to the phonon anharmonicity.

Thermal conductivity

The Slack's approach does not take into account the underlying phonon scattering mechanisms and is mostly

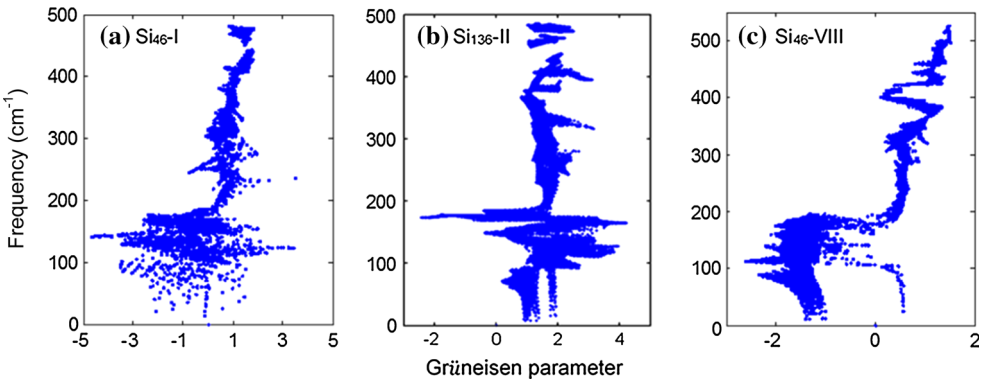

Fig. 5 Mode Grüneisen parameter for studied Si clathrates. Each dot represents a phonon mode at a q point

Table 3 The parameters of the Slack's formula such as $\overline{M}$ (average atomic mass), δ (the average volume per atom), n (the number of atoms in primitive cell), θ_D (Debye temperature), and γ (weighted average Grüneisen parameter) along with the sound velocities and elastic constants for Si_{46}-I, Si_{136}-II, and Si_{46}-VIII clathrates. All the parameters were obtained from this study

	$\overline{M}$ (amu)	δ (Å)	n	θ_D (K)	γ	v_l (m/s)	v_t (m/s)	C_{11} (GPa)	C_{12} (GPa)	C_{44} (GPa)
Si_{46}-I	28.0855	2.8548	46	550	1.5	8244	4746	130.9	48.7	48.2
Si_{136}-II	28.0855	2.8665	34	519	1.65	8185	4450	143	53.3	38
Si_{46}-VIII	28.0855	3.552	23	549	1.29	8011	4557	139.3	46.3	42.3

based on the Grüneisen parameter as a measure of anharmonicity, Debye temperature and the number of atoms in the unit cell. Table 3 presents all input parameters for the Slack's formula. All the parameters shown in this table were obtained from this study. Our calculated Debye temperatures are in excellent agreement with previous theoretical study [29] in which reports values of 551 and 516 K, respectively, for Si_{46}-I, and Si_{136}-II clathrates. The average atomic masses for the studied materials are the same and the Debye temperatures are almost equal. Therefore, the average volume per atom, the number of atoms in the primitive cell and the Grüneisen parameter contribute the most in the thermal conductivity. According to the Slack's formula, the thermal conductivity depends directly to the δ and inversely to the γ^2 and $n^{2/3}$. So, the thermal conductivity should decrease as the average volume per atom decreases or the number of atoms in primitive cell and Grüneisen parameter increase.

Figure 7 illustrates the calculated thermal conductivities of studied Si clathrates using Slack's formula. It shows that the lowest thermal conductivity belongs to the type-II Si clathrate material while the highest one belongs to the type-VIII Si clathrate. The thermal conductivity values of Si_{46}-I, Si_{136}-II, and Si_{46}-VIII clathrates at room temperature are 4.9, 4.1, and 13.5 W/m–K, respectively. It is also notable that the thermal conductivity curves of Si_{46}-I and Si_{136}-II clathrates are very close to each other. The discrepancy between measured (2.5 W/m–K at room temperature [34]) and calculated values of thermal conductivity for Si_{136}-II can be attributed to the effect of grain boundary, impurities, and defects scatterings in which are existent in material samples and can significantly lower the thermal conductivity.

The calculated thermal conductivities are very low and in case of Si_{46}-I, Si_{136}-II structures approach to the amorphous limit at higher temperature. Such a small thermal conductivity can be attributed to the relatively high amount of the phonon anharmonicity, and complex structure of unit cells. Such a suppression of thermal conductivity by the phonon anharmonicity has been already reported for type-I clathrates [35].

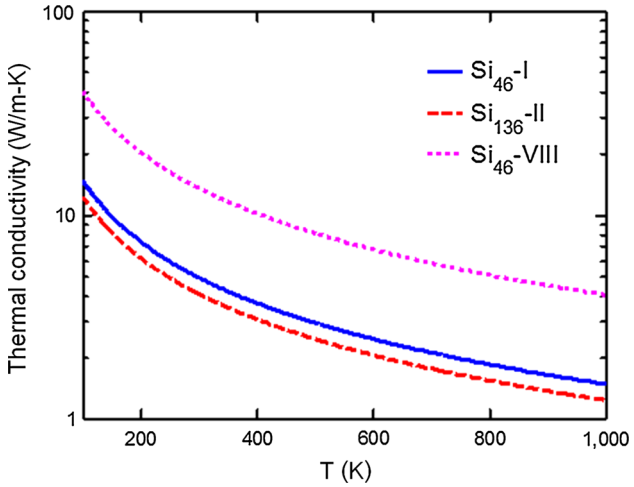

Fig. 7 The calculated thermal conductivities of studied silicon clathrates using Slack's formula

Thermoelectric efficiency

To the best of our knowledge, there is no report in literature containing measured or calculated values of electrical properties such as electrical conductivity and Seebeck coefficient for clathrates Si_{46}-I and Si_{136}-II. However, our previous study based on DFT calculations revealed a large number of closely packed electron pockets near both the conduction and valance band edges [36]. Such an extraordinary bandstructure is mostly desired for TE applications. The large number of band degeneracy is predicted to generate large Seebeck coefficient and the high band curvature would cause low conductivity effective mass; hence, a high carrier mobility. Both such properties favor the enhancement of the TE power factor. We expect that the parental Si_{46}-VIII should make available a favorable starting material in search of Si-based TE materials. The intercalation of the pristine Si_{46}-VIII with a guest atom would introduce opportunity for concurrent reduction of the thermal conductivity and improvement of the TE power factor, which has been indeed a tough challenge in designing efficient TE materials. We have already predicted an extraordinarily large power factor for clathrate Si_{46}-VIII [37]. Moreover, the electronic structure of alkali

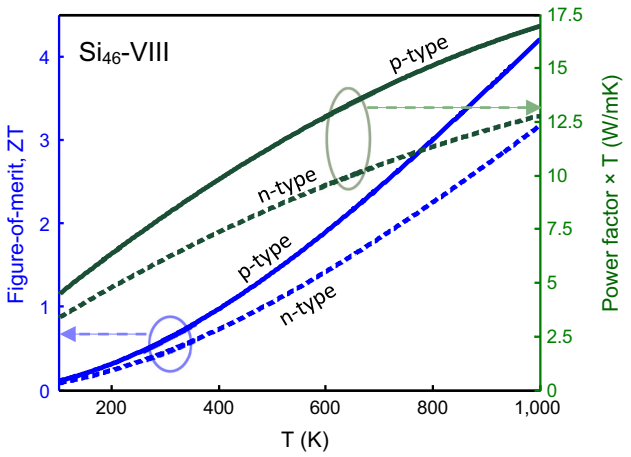

Fig. 8 Figure-of-merit and thermoelectric power factor (PFT) versus temperature for both p-type and n-type Si_{46}-VIII materials at a doping concentration of 1.1×10^{21} cm^{-3}

and alkaline-earth intercalated type-VIII Si clathrates have been investigated and potential large power factors due to the existence of a large number of carrier pockets near their band edges were predicted [38]. We utilized our own calculated results in Ref. [37] and the calculated thermal conductivity based on the Slack's formula to estimate the figure-of-merit ZT for both p-type and n-type clathrates Si_{46}-VIII materials. We have neglected the contribution of charge carriers into the total thermal conductivity. Figure 8 demonstrates the calculated values of ZT (left vertical axis) and power factor multiplied by T (right vertical axis) versus temperature for both p-type and n-type Si_{46}-VIII clathrate materials at a doping concentration of 1.1×10^{21} cm^{-3}. The blue and green curves are corresponding to values of ZT and PFT, respectively. Each curve has been labeled by p-type or n-type to indicate the type of carrier concentration.

Figure 8 shows that in both p-type and n-type Si_{46}-VIII materials ZT increases as temperature raises. The predicted ZT at room temperature for p-type and n-type Si_{46}-VIII materials are, respectively, $\sim$0.6 and $\sim$0.45. It should be noted that the clathrate Si_{46}-VIII is a parental material and its TE performance can be enhanced by well-established techniques for reducing the thermal conductivity or improving the power factor.

Summary and conclusion

We have performed first-principles lattice dynamical calculations based on density functional theory on Si_{46}-I, Si_{136}-II, Si_{46}-VIII materials and analyzed their structural stability, possibility of pressure-driven or temperature-driven phase transitions, and the degree of phonon anharmonicity through evaluation of three properties such as Grüneisen parameter, coefficient of thermal expansion, and thermal conductivity. For this purpose, we conducted lattice dynamic calculations using DFT and calculated the volume-dependent free energies within QHA. The relatively high Grüneisen parameters, and very low thermal conductivities along with the existence of negative region in thermal expansion coefficients of studied Si clathrates; all can be attributed to the highly anharmonic phonon interactions. These results implicate that the optical phonons could have a significant role in scattering acoustic phonons through anharmonic phonon interactions. The calculated low thermal conductivities of studied pristine silicon clathrates would open road for designing high performance Si-based TE materials.

Acknowledgements The authors would like to thank the Texas Tech High Performance Computing Center for many hours of computing time.

References

1. Slack GA (1995) In: Rowe DM (ed) CRC Handbook of Thermoelectrics. CRC, Boca Raton
2. Härkönen VJ, Karttunen AJ (2014) Ab initio lattice dynamical studies of silicon clathrate frameworks and their negative thermal expansion. Phys Rev B 89:024305
3. Ashcroft NW, Mermin ND (1976) Solid State Physics. HRW International Editions, CBS Publishing Asia Ltd., Philadelphia
4. Fujiwara A, Sugimoto K, Shih CH, Tanaka H, Tang J, Tanabe Y, Xu J, Heguri S, Tanigaki K, Takata M (2012) Quantitative relation between structure and thermal conductivity in type-I clathrates $X_8Ga_{16}Ge_{30}$ (X = Sr, Ba) based on electrostatic-potential analysis. Phys Rev B 85:144305
5. Suekuni K, Takasu Y, Hasegawa T, Ogita N, Udagawa M, Avila MA, Takabatake T (2010) Off-center rattling modes and glasslike thermal conductivity in the type-I clathrate $Ba_8Ga_{16}Sn_{30}$. Phys Rev B 81:205207
6. Zheng X, Rodriguez SY, Ross JH Jr (2011) NMR relaxation and rattling phonons in type-I $Ba_8Ga_{16}Sn_{30}$ clathrate. Phys Rev B 84:024303
7. Sales BC, Chakoumakos BC, Jin R, Thompson JR, Mandrus D (2001) Structural, magnetic, thermal, and transport properties of X8Ga16Ge30 (X = Eu, Sr, Ba) single crystals. Phys Rev B 63:245113
8. Suekuni K, Avila MA, Umeo K, Fukuoka H, Yamanaka S, Nakagawa T, Takabatake T (2008) Simultaneous structure and carrier tuning of dimorphic clathrate $Ba_8Ga_{16}Sn_{30}$. Phys Rev B 77:235119
9. Slack GA (1979) In: Ehrenreich H, Seitz F, Turnbull D (eds) Solid State Physics, vol 34. Academic Press, New York, p 1
10. Nolas GS, Slack GA, Schujman SB (2001) In: Tritt TM (ed) Semiconductors and Semimetals. Academic Press, San Diego
11. Beekman M, Nolas GS (2008) Inorganic clathrate-II materials of group 14: synthetic routes and physical properties. J Mater Chem 18:842
12. Martin J, Erickson S, Nolas GS, Alboni P, Tritt TM, Yang J (2006) Structural and transport properties of $Ba_8Ga_{16}Si_xGe_{30-x}$ clathrates. J Appl Phys 99:044903
13. Giannozzi P, Baroni S, Bonini N, Calandra M, Car R, Cavazzoni C, Ceresoli D, Chiarotti GL, Cococcioni M, Dabo I (2009)

QUANTUM ESPRESSO: a modular and open-source software project for quantum simulations of materials. J Phys 21:395502
14. Perdew JP, Burke K, Ernzerhof M (1996) Generalized Gradient Approximation Made Simple. Phys Rev Lett 77:3865
15. Troullier N, Martins JL (1990) A Straightforward Method for Generating Soft Transferable Pseudopotentials. Solid State Commun 74:613
16. Kleinman L, Bylander DM (1982) Efficacious Form for Model Pseudopotentials. Phys Rev Lett 48:1425
17. Monkhorst HJ, Pack JD (1976) Special points for Brillouin-zone integrations. Phys Rev B 13:5188
18. Baroni S, Resta R (1986) Ab initio calculation of the macroscopic dielectric constant in silicon. Phys Rev B 33:7017
19. Baroni S, Giannozzi P, Testa A (1861) Green's-function approach to linear response in solids. Phys Rev Lett 1987:58
20. Alfe D (2009) PHON: a program to calculate phonons using the small displacement method. Comput Phys Commun 180:2622
21. Methfessel M, Paxton AT (1989) High-precision sampling for Brillouin-zone integration in metals. Phys Rev B 40:3616
22. Tang X, Dong J, Hutchins P, Shebanova O, Gryko J, Barnes P, Cockcroft JK, Vickers M, McMillan PF (2006) Thermal properties of Si_{136}: theoretical and experimental study of the type-II clathrate polymorph of Si. Phys Rev B 74:014109
23. Fultz B (2010) Vibrational thermodynamics of materials. Prog Mater Sci 55:247
24. Gurevich VL, Parshin DA, Schober HR (2003) Anharmonicity, vibrational instability, and the Boson peak in glasses. Phys Rev B 67:094203
25. Broido DA, Ward A, Mingo N (2005) Lattice thermal conductivity of silicon from empirical interatomic potentials. Phys Rev B 72:014308
26. Narasimhan S, de Gironcoli S (2002) Ab initio calculation of the thermal properties of Cu: performance of the LDA and GGA. Phys Rev B 65:064302
27. Smith TF, Birch JA, Collins JG (1976) Low-temperature heat capacity, thermal expansion and Gruneisen parameters for SnTe. J Phys C 9(24):4375
28. Julian CL (1965) Theory of Heat Conduction in Rare-Gas Crystals. Phys Rev 137:A128
29. Connétable D (2010) First-principles calculations of carbon clathrates: Comparison to silicon and germanium clathrates. Phys Rev B 82(7):075209
30. Moriguchi K, Munetoh S, Shintani A, Motooka T (2001) Empirical potential description of energetics and thermodynamic properties in expanded-volume silicon clathrates. Phys Rev B 64(19):195409
31. Saito S, Oshiyama A (1995) Electronic structure of Si 46 and Na 2 Ba 6 Si 46. Phys Rev B 51(4):2628
32. Giannozzi P, de Gironcoli S, Pavone P, Baroni S (1991) Ab initio calculation of phonon dispersions in semiconductors. Phys Rev B 43:7231
33. Maradudin AA, Montroll EW, Weiss GH, Ipatva IP (1971) Theory of lattice dynamics in the harmonic approximation, 2nd edn. Academic press, New York
34. Nolas GS, Beekman M, Gryko J, Lamberton GA, Tritt TM, McMillan PF (2003) Thermal conductivity of elemental crystalline silicon clathrate Si_{136}. Appl Phys Lett 82:6
35. Wu J, Xu J, Prananto D, Shimotani H, Tanabe Y, Heguri S, Tanigaki K (2014) Systematic studies on anharmonicity of rattling phonons in type-I clathrates by low-temperature heat capacity measurements. Phys Rev B 89:214301
36. Norouzzadeh P, Myles CW, Vashaee D (2013) Prediction of a large number of electron pockets near the band edges in type-VIII clathrate Si_{46} and its physical properties from first principles. J Phys 25(47):475502
37. Norouzzadeh P, Myles CW, Vashaee D (2014) Prediction of Giant Thermoelectric Power Factor in Type-VIII Clathrate Si_{46}. Sci Rep 4:7028
38. Norouzzadeh P, Krasinski JS, Myles CW, Vashaee D (2015) Type-VIII Si based clathrates: prospects for a giant thermoelectric power factor. Phys Chem Chem Phys 17(14):8850–8859